CHIN. PHYS. LETT. Vol. 37, No. 7 (2020) 074502

Evolution of Energy in Submerged Granular Column Collapse

Wen-Tao Zhang(张炆涛)[1,2], Yi An(安翼)[2], Qing-Quan Liu(刘青泉)[3*],
Xiao-Liang Wang(王晓亮)[3], and Yun-Hui Sun(孙云辉)[3]

[1]*School of Engineering Sciences, University of Chinese Academy of Sciences, Beijing 100049, China*
[2]*Institute of Mechanics, Chinese Academy of Sciences, Beijing 100190, China,*
[3]*Department of Mechanics, Beijing Institute of Technology, Beijing 100081, China*

(Received 6 March 2020; accepted 14 May 2020; published online 21 June 2020)

The evolution of energy in subaerial and subaqueous granular column collapses is studied. Employing the refractive index matching method and planar laser-induced fluorescence technique, we obtain granular and liquid images simultaneously in a single experiment of subaqueous flow. Particle image velocimetry and particle tracking velocimetry are used to process the data for the fluid and granular phase. We find stepwise decreases in the total kinetic energy of the granular material. The stage of rapidly falling energy corresponds to large transverse changes in the direction of the massive granular particles. Moreover, in this stage, a major fraction of the granular kinetic energy transferred from the granular potential energy is lost or transferred. Interestingly, compared with dry granular flow, the existence of an ambient liquid seems to reduce the total dissipated energy, which may be the reason why previous studies observed similar granular runout distances in subaqueous and dry granular collapses.

PACS: 45.70.Mg, 47.55.Kf, 47.57.Gc DOI: 10.1088/0256-307X/37/7/074502

Submarine avalanches, turbidity currents, and debris flow are three examples of granular-liquid mixture flow phenomena that have widespread occurrence in nature. These geophysical mass flows differ from others such as rock avalanches because they contain solid particles and fluid, both phases playing significant roles on the flow dynamics. Although the theory concerning dry granular flows has developed rapidly, the effects of ambient fluid on granular flow dynamics are still poorly understood.[1] Water exerts much greater drag than air, and buoyancy decreases the effect of gravity acting on granular media; in addition, water dissipates energy through its viscosity. However, Heim's ratio of subaqueous rock avalanches is not larger than that of equi-voluminous granular avalanches without ambient water.[2,3] The runout distance of granular collapse in a fluid may be similar to that of dry granular collapse.[4] In both situations, excess pore pressure[5] and hydroplaning[2] play no role because the particles are coarse. Therefore, other mechanisms must be present to explain this behavior.

To further understand the role of ambient fluid on the dynamics of granular flows, we study the evolution of the energy in granular column collapses with and without ambient liquid. Submerged and dry granular column collapses were investigated in experiments and discrete element method (DEM) simulations. For the present study, the experiments were performed in a transparent glass box of 500 mm length, 96 mm height, and 4.61 mm width, which is about 1.2 times the granular diameter, and determined by the placement of two glass partitions. An initial granular pile was formed behind a stainless-steel wire of 3 mm diameter to one side of the box. The initial granular pile had fixed dimensions of $l_0 \times w \times h_0 = 43 \times 4.61 \times 82\,\text{mm}^3$, providing an aspect ratio of $a = h_0/l_0 = 1.9$. In total, 243 particles were packed. The steel wire threaded a rubber plug, which was fixed to a glass pane on top of the glass box to ensure the wire to be removed vertically. Having prepared the granular column, the glass box was filled with liquid. Another glass pane was then placed on top of the glass box to avoid impulsive waves on the free surface. In the submerged case, a continuous wave laser was placed on the opposing side of the glass box to provide a green laser sheet (532 nm, 10 W) at the widthwise central plane. The thickness of the laser sheet was less than 0.5 mm in the observational range. The illuminated region is shown in Fig. 1(b). In the dry case, an LED was used instead. The experiment commenced with the stainless-steel wire being removed abruptly away from the granular pile, thereby beginning the collapse of the granular pile. The whole process was recorded with a high-speed camera at a rate of 1080 frames per second with 2048 × 2048 pixels per frame. The spatial resolution was about 13.2 pixels/mm. The experimental configuration for submerged granular column collapse is shown in Fig. 1.

Supported by the National Natural Science Foundation of China (Grant Nos. 11872117, 11672310, and 11602278), and the National Key Research and Development Program of China (Grant No. 2016YFC0303708).
*Corresponding author. Email: liuqq@bit.edu.cn
© 2020 Chinese Physical Society and IOP Publishing Ltd

The granular medium used in the experiment comprised of borosilicate glass beads of diameter $d = 3.84\,\text{mm}$ and polydispersity of 8%. The granular density ρ_s is $2178\,\text{kg/m}^3$ and granular refractive index n_s is 1.474. A mixture of dimethyl sulfoxide (DMSO) and water was used to match this refractive index. The mixture has density $\rho_\text{f} = 1087\,\text{kg/m}^3$, viscosity $2.37 \times 10^{-3}\,\text{Pa·s}$, and a refractive index $n_\text{f} = 1.474$. To obtain information regarding the liquid flow field, small fluorescent tracer particles that respond strongly to laser illumination were added to the liquid phase. Then, a small amount of rhodamine 6G was added to achieve a good contrast between liquid and glass beads under laser illumination. The concentration of rhodamine 6G was chosen to make the brightness of the liquid less than that of the tracer particles. A 550-nm-long pass optical filter was used to block the emission from the laser sheet but allowed the emission from the fluorescence to remove minor reflections from the glass sphere surfaces and from the glass-box walls.

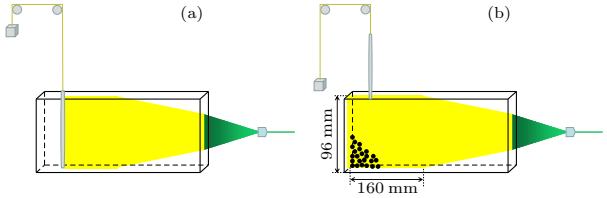

Fig. 1. A sketch of the experimental setup used for submerged granular column collapse: (a) before the beginning of granular column collapse, the particle is invisible, and (b) after lifting the stainless-steel wire, the granular pile begins to collapse.

We used the circular Hough transform to obtain the position and radius of the circles in the laser sheet. Because each single granular displacement in three time steps was still smaller than the interparticle spacing, nearest-neighbor matching was used to track particles. Considering that a few particles went occasionally undetected and particles may have appeared and disappeared through successive frames, the criterion $\delta r_i^{(n1)} > d$ was deemed a bad particle association. In this study, $\delta r_i^{(nk)}$ represents the distance between particle i at time $t^{(n)}$ and its nearest neighbor at time $t^{(n+k)}$ with $k = 123$. Next, we computed $\delta r_i^{(n2)}$ and $\delta r_i^{(n3)}$ in that order. If $\delta r_i^{(n2)} > d$ and $\delta r_i^{(n3)} > d$, we would assume that we had lost track of particle i after time $t^{(n)}$. A particle not associated with any track was given with a new id label. If the particle was being tracked, the granular velocities can be calculated by

$$\boldsymbol{v}_{pi}^{(n)} = \frac{\boldsymbol{r}_i^{(n+l)} - \boldsymbol{r}_i^{(n)}}{l\Delta t}, \tag{1}$$

where $r_i^{(n)} = (x_i^{(n)} y_i^{(n)})$ denotes the position of particle i at time $t^{(n)}$ (the x and y axes are oriented in directions parallel and perpendicular to the bottom of the glass box), and $\boldsymbol{v}_{pi}^{(n)} = (u_{pi}^{(n)} v_{pi}^{(n)})$ the granular velocity of particle i in the laser sheet.

PIVlab[6] was used to determine the velocity of the liquid phase, we chose the discrete Fourier transform (DFT), which is calculated using the fast Fourier transform (FFT) to solve the discrete cross-correlation function. A two-pass approach was used to increase the spatial resolution without loss of pair errors for large displacements.[7] The interrogation windows of the first and second pass were set to 64 pixels × 64 pixels and 32 pixels × 32 pixels, respectively, both with 50% overlaps. The location of the intensity peak of the correlation matrix was refined with subpixels using the Gauss 2×3-point fit method. The computed liquid velocity would be regarded as an outlier if it lay outside the range of the velocity thresholds. The upper and lower thresholds are given by

$$v_\text{upper} = \bar{v} + n\sigma, \tag{2}$$

$$v_\text{lower} = \bar{v} - n\sigma, \tag{3}$$

where $\bar{v}$ denotes the mean velocity, σ the standard deviation of v; n is set to 7 for this study. The outliers are removed and replaced by interpolated data, which are obtained from a boundary value solver.[6]

As for dry granular column collapse, the DEM open source code LIGGGHTS is employed[8] for numerical simulation. Apart from granular density and diameter mentioned above, other required parameters are Young's modulus E, Poisson's ratio σ, the coefficient of interparticle friction (μ_c), the coefficient of Coulomb friction between the particle and wall (μ_w), and the coefficient of restitution (e). The value of E for borosilicate glass is about $6.4 \times 10^{10}\,\text{Pa}$. However, to save computational time, we set $E = 6.4 \times 10^7\,\text{Pa}$, which has no influence on flow characteristics.[9] The value of Poisson's ratio of borosilicate glass was set to $\sigma = 0.2$. Because the typical yield stress ratio for monodisperse glass beads is 0.38,[1] this value corresponds to $\mu_\text{c} = 0.5$.[10] For the coefficient μ_w, the value measured by Foerster *et al.*[11] was adopted ($\mu_\text{w} = 0.125$). Finally, the coefficient of restitution has been demonstrated to have little influence on granular column collapse, except for extreme unrealistic instances when $e = 1$.[12] In this study, we chose the same value as Cleary and Frank for the coefficient of restitution ($e = 0.4$).

Figure 2 shows the experimental and DEM simulated results of the final deposit of granular column collapses with an aspect ratio of 2.0. The runout distances are 140 mm in submerged situation, 145 mm in dry experiment and 140 mm in DEM simulation. Here, the final runout distance is defined by the position of the farthest particles from the center of the initial granular column with a minimum of one contact

with the main deposit, which is consistent with the definition by Lacaze *et al.*[13] and Kermani *et al.*[14] We found that the runout distance of granular column collapse is similar in submerged and dry situations and this is the consistent with the result obtained by Topin through their 2D DEM-CFD simulation.[4] We also found that the evolution of energy is nearly the same in the dry experiment and DEM simulation (results are omitted due to the page limitation). Considering the DEM result could recognize the step of energy evolution, which is an important focus in this study, more distinctly, the following discussion of dry granular column collapse is based on DEM simulation results.

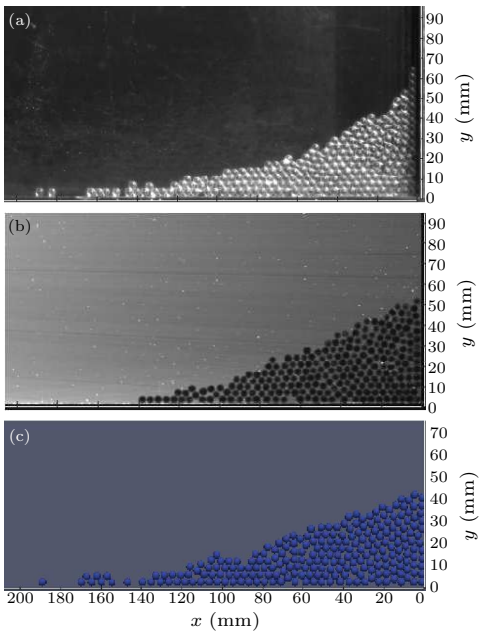

Fig. 2. (a) Final deposit of dry column collapse experiment, (b) final deposit of submerged column collapse experiment, (c) final deposit of DEM result.

To get a deeper understanding of this phenomenon, we study the energy evolution of granular column collapse in both dry and submerged situations. With the granular position, velocity, and liquid velocity being calculated at every time step, we can then determine the time evolution of the energy. The kinetic energy of the granular phase in the horizontal and vertical directions is calculated from

$$E_{kx}^{\mathrm{p}}(t^{(n)}) = \frac{1}{2}\sum_{i=1}^{N_{\mathrm{p}}^{(n)}} m_i (u_{pi}^{(n)})^2, \tag{4}$$

$$E_{ky}^{\mathrm{p}}(t^{(n)}) = \frac{1}{2}\sum_{i=1}^{N_{\mathrm{p}}^{(n)}} m_i (v_{pi}^{(n)})^2, \tag{5}$$

where $E_{kx}^{\mathrm{p}}(t^{(n)})$ and $E_{ky}^{\mathrm{p}}(t^{(n)})$ are the respective horizontal and vertical kinetic energies of the particles at time $t^{(n)}$, with m_i the mass of particle i and $N_{\mathrm{p}}^{(n)}$ the total number of detected particles at time $t^{(n)}$, although maybe one or two particles are not detected in few frames, it does not affect our conclusion. The total kinetic energy of the granular phase is their sum,

$$E_k^{\mathrm{p}}(t^{(n)}) = E_{kx}^{\mathrm{p}}(t^{(n)}) + E_{ky}^{\mathrm{p}}(t^{(n)}). \tag{6}$$

Note that the rotational kinetic energy was omitted in this study as it had been found to be negligible in comparison with the translational energies during granular collapses.[15] The total granular potential energy E_{p} and the reduced potential energy E'_{p} are defined as

$$E_{\mathrm{p}}(t^{(n)}) = \sum_{i=1}^{N_{\mathrm{p}}^{(n)}} m_i g h_i^{(n)}, \tag{7}$$

$$E'_{\mathrm{p}}(t^{(n)}) = \sum_{i=1}^{N_{\mathrm{p}}^{(n)}} m_i g' h_i^{(n)}, \tag{8}$$

where g denotes the acceleration due to Earth's surface gravity, $g' = (\rho_{\mathrm{p}} - \rho_{\mathrm{f}})g/\rho_{\mathrm{p}}$ represents the effective gravity, and $h_i^{(n)}$ denotes the relative height between the center of the i^{th} particle and the bottom of the glass box at time $t^{(n)}$. The initial potential energy of the granular column before particles start to move was calculated using

$$E_0 = \sum_{i=1}^{N_{\mathrm{p}}} m_i g h_0/2, \tag{9}$$

$$E'_0 = \sum_{i=1}^{N_{\mathrm{p}}} m_i g' h_0/2, \tag{10}$$

where N_{p} is the total number of particles in the granular column. Next, we determined the reduction in the potential energy of the granular phase,

$$\Delta E_{\mathrm{p}} = E_0 - E_{\mathrm{p}}(t^n), \tag{11}$$

$$\Delta E'_{\mathrm{p}} = E'_0 - E'_{\mathrm{p}}(t^n). \tag{12}$$

For calculation of the kinetic energy of the liquid phase, we need the widthwise velocity distribution of the liquid. However, we measured instead the widthwise liquid velocity at the central plane. Given the maximal liquid velocity V_{m} during granular column collapse is about 0.3 m/s, the maximal Reynolds number of the liquid phase is $\mathrm{Re}_{\mathrm{m}} = \rho_{\mathrm{f}} V_{\mathrm{m}} W/2\mu_{\mathrm{f}} \approx 317$. The value is well below the critical Reynolds number for planar Poiseuille flow.[16] Therefore, we assumed the flow to be laminar and the widthwise velocity distribution of the liquid to be parabolic. The kinetic energy of the liquid phase both horizontally and vertically are

$$E_{kx}^{\mathrm{f}}(t^{(n)}) = \frac{1}{2} V_{\mathrm{f}} \sum_{i=1}^{N_{\mathrm{f}}} \rho_{\mathrm{f}} \left(\frac{2}{3} u_{fi}^{(n)}\right)^2, \tag{13}$$

$$E_{ky}^{\mathrm{f}}(t^{(n)}) = \frac{1}{2} V_{\mathrm{f}} \sum_{i=1}^{N_{\mathrm{f}}} \rho_{\mathrm{f}} \left(\frac{2}{3} v_{fi}^{(n)} \right)^2, \tag{14}$$

where V_{f} denotes the volume of the liquid cell, the size of which is 2.42 mm ×4.61 mm ×2.42 mm, based on the size of the interrogation windows used in particle image velocimetry (PIV), N_{f} the total number of the liquid cells, and $u_{fi}^{(n)}$ and $v_{fi}^{(n)}$ denote the measured central liquid velocities of the ith liquid cell in the horizontal and vertical directions at time $t^{(n)}$. The total kinetic energy of liquid phase is then

$$E_k^{\mathrm{f}}(t^{(n)}) = E_{kx}^{\mathrm{f}}(t^{(n)}) + E_{ky}^{\mathrm{f}}(t^{(n)}). \tag{15}$$

The energy dissipated in the flow at any given time is approximately

$$E_d(t^{(n)}) = \Delta E_{\mathrm{p}}' - E_k^{\mathrm{p}} - E_k^{\mathrm{f}}. \tag{16}$$

Figures 3(a)–3(d) show the normalized reduction of the potential energy of the granular phase, the dissipated energy, the granular kinetic energy, and the liquid kinetic energy (if applicable) for both dry and submerged collapses, respectively. We found the evolution of energy for both dry and submerged situations to be similar; indeed, about 55% of the initial potential energy is dissipated in the whole dynamic process. The kinetic energy of the granular phase increases to its peak at around 1.25 times the characteristic time, and then reduces to zero at around 5. The kinetic energy in the horizontal direction reaches its peak later than that in the vertical direction. However, the maximal granular kinetic energy ratio during granular column collapse for submerged flows is half that for dry flows; the maximal liquid kinetic energy $E_{\mathrm{k,max}}^{\mathrm{f}}$ is about one fifth of $E_{\mathrm{k,max}}^{\mathrm{p}}$. This is surprising because the particles are transported almost with the same distance in dry and submerged flows, whereas the supplied granular kinetic energy in the submerged flows is much less. To find the reason, we studied the difference in granular kinetic energy dissipative mechanisms between the submerged and dry flows. We found that the reduction of the granular kinetic energy is not gradual but step-like (Fig. 3). The cause of this step-wise change in granular kinetic energy is revealed in the granular trajectory. We found the trajectory of a massive granular particle also to be step-like, which is different from the quasi-static avalanche process of a granular pile,[17] and the granular kinetic energy is likely to be related to the mode of granular motion. The stage of rapid decline in granular kinetic energy may correspond to the stage in which many particles are undergoing inelastic collisions, and their direction of motion changes laterally.

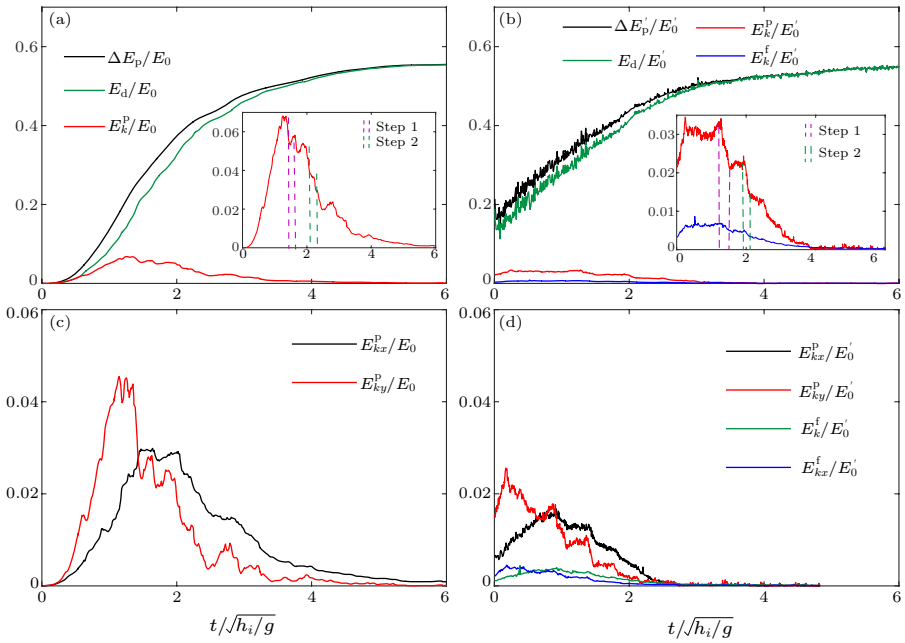

Fig. 3. Evolution of the energy [(a), (b)] and kinematic energy ratio [(c), (d)] for dry [(a), (c)] and submerged [(b), (d)] situations.

To support this hypothesis, we studied the trajectory of particles during this rapid decline in granular kinetic energy. Indeed, most particles for which the kinetic energy decreased significantly undergo sharp changes in direction from a falling motion to a lateral motion. Typical granular trajectories during steps 1 and 2 are shown in Fig. 4. Because the steep decrease in granular kinetic energy is mainly due to granular impacts, this dissipated energy does not assist in the transport of particles, implying that the more gran-

ular kinetic energy is involved in this rapid decline, the less granular kinetic energy is available for transporting particles. In submerged and dry granular collapses, the respective ratios of the total granular kinetic energy in the rapid decline stage to the maximal granular kinetic energy are 0.76 and 0.91.

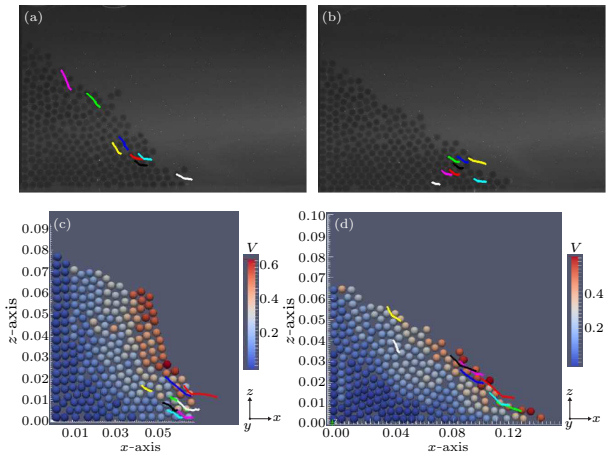

Fig. 4. Tracks of eight typical particles for which the kinetic energy decreases significantly in two rapid-decrease energy phases: (a) step 1 in the immersed case, (b) step 2 in the immersed case, (c) step 1 in the dry case, and (d) step 2 in the dry case.

In summary, we have confirmed that the presence of ambient liquid in submerged flows does not necessarily shorten the runout distance of the granular column collapse compared with the dry situation. Nevertheless, ambient fluid definitely reduces the releasable potential energy of particles and may dissipate more energy. We found that the granular kinetic energy obtained declines with time in a step-wise manner, and that the trajectories of the active particles show sharp lateral changes, simultaneously. The rapid decline in the kinetic energy exhibited by the granular system corresponds to a stage in which falling trajectories of massive granular particles become lateral. This means that a large percentage of the kinetic energy the granular system obtains dissipates or is transferred laterally. For subaqueous and dry granular column collapses, 76% and 91%, respectively, of the maximal granular kinetic energy is dissipated in this way. For subaqueous flows, the lower percentage of the dissipated energy in this stage may be due to the fact that the runout distance of the granular flow is similar to dry flows as this dissipated energy does not contribute to the transport of particles. This may explain the non-intuitive granular flow runout phenomenon.

References

[1] Andreotti T B, Forterre Y and Pouliquen O 2013 *Granular Media: Between Fluid and Solid* (Cambridge: Cambridge University Press)
[2] De Blasio F V 2011 *Introduction to the Physics of Landslides* (Berlin: Springer)
[3] Lucas A, Mangeney A and Ampuero J P 2014 *Nat. Commun.* **5** 3417
[4] Topin V, Monerie Y, Perales F *et al.* 2012 *Phys. Rev. Lett.* **109** 188001
[5] Iverson R M and George D L 2014 *Proc. R. Soc. A* **470** 20130819
[6] Thielicke W and Stamhuis E J 2014 *J. Open Res. Software* **2** e30
[7] Sarno L, Carravetta A, Tai Y C *et al.* 2018 *Adv. Powder Technol.* **29** 3107
[8] Kloss C, Goniva C, Hager A *et al.* 2012 *Prog. Comput. Fluid Dynam.* **12** 140
[9] Girolami L, Hergault V, Vinay G *et al.* 2012 *Granul. Matter* **14** 381
[10] Berzi D and Vescovi D 2015 *Phys. Fluids* **27** 013302
[11] Foerster S F, Louge M Y, Chang H *et al.* 1994 *Phys. Fluids* **6** 1108
[12] Staron L and Hinch E J 2005 *J. Fluid Mech.* **545** 1
[13] Lacaze L, Phillips J C and Kerswell R R 2008 *Phys. Fluids* **20** 063302
[14] Kermani E, Qiu T and Li T 2015 *Int. J. Geomech.* **15** 04015004
[15] Utili S, Zhao T and Houlsby G T 2015 *Eng. Geol.* **186** 3
[16] Nishioka M, Iida S and Ichikawa Y 1975 *J. Fluid Mech.* **72** 731
[17] Pan B C, Shi Q F and Sun G 2013 *Chin. Phys. Lett.* **30** 124701